Catalysis Communications 84 (2016) 175–178

Contents lists available at ScienceDirect

Catalysis Communications

journal homepage: www.elsevier.com/locate/catcom

Short Communication

Effect of impregnation sequence on performance of SiO_2 supported Cu-Fe catalysts for higher alcohols synthesis from syngas

Chao Sun, Dongsen Mao *, Lupeng Han, Jun Yu

Research Institute of Applied Catalysis, School of Chemical and Environmental Engineering, Shanghai Institute of Technology, Shanghai 201418, PR China

ARTICLE INFO

Article history:
Received 24 March 2016
Received in revised form 20 June 2016
Accepted 4 July 2016
Available online 05 July 2016

Keywords:
Cu-Fe/SiO_2
CO hydrogenation
Higher alcohols
Impregnation sequences

ABSTRACT

The effects of different impregnation sequences of copper and iron on the performance of Cu-Fe/SiO_2 catalysts for higher alcohols synthesis from syngas were investigated by N_2 adsorption, XRD, H_2-TPR, CO-IR, XPS, and CO hydrogenation reaction. The results indicate that the catalyst prepared by impregnation of support first with Fe and then with Cu exhibits the highest selectivity (36.1%) and space time yield (153.3 $g \cdot kg_{cat}^{-1} \cdot h^{-1}$) of alcohols. The CO conversion and alcohol selectivity of the catalysts was closely related to the content of surface Cu, and the ratio of surface contents of Cu to Fe, respectively.

1. Introduction

Higher alcohols synthesis (HAS) from syngas derived from coal, natural gas, and biomass has attracted more and more attention. Several effective catalytic systems have been developed for HAS up to date, which include modified methanol synthesis catalysts, MoS_2-based catalysts, modified Fischer–Tropsch (F-T) catalysts and Rh-based catalysts [1–3]. Among them, the Cu-Fe based catalyst is considered as one of the most promising catalysts due to low cost, high catalytic performance and selectivity of higher alcohols, and high water-gas shift (WGS) activity [4–6]. Although numerous studies have been performed with the Cu-Fe based catalysts [4–27], there are still many problems to be solved, such as the formation of byproducts like hydrocarbons and CO_2, the low selectivity of higher alcohols [9,13,14,25]. So, how to further improve the performance of the Cu-Fe-based catalysts for HAS remains a topic for future study.

It is well known that, for a supported multi-component catalyst, the introduction sequence of the different components may affect the interaction and dispersion of different components, thus affecting the catalytic performance. For example, Deng et al. [28] found that the impregnation order significantly affected the microstructure and performance of Cu-Co/SiO_2 catalyst for the synthesis of higher alcohols. Wang et al. [29] and Yu et al. [30] reported that the sequences of introducing the Fe promoter exhibited great effect on the activity and selectivity of the Rh/SiO_2-based catalysts for the synthesis of ethanol. Borer et al. [31] and Liu et al. [32] found that the impregnation sequence affected the performance of lanthana promoted Rh/SiO_2 and ceria promoted Rh-Fe/SiO_2 catalysts, respectively.

In this paper, three SiO_2 supported Cu-Fe catalysts were prepared by different impregnation methods, and used for the synthesis of higher alcohols from syngas. In order to elucidate the influence of the impregnation method, the physicochemical properties of the catalysts were characterized by XRD, N_2 adsorption, H_2-TPR, CO-IR, and XPS techniques.

2. Experimental

2.1. Catalyst preparation

A commercial silica gel (Qingdao Haiyang Chemicals Company, China) was pretreated following previously reported procedure [22] and used as the support in this study.

Co-impregnation and sequential impregnation methods were employed for the preparation of SiO_2 supported Cu-Fe catalysts; both the Cu and Fe loadings of the catalysts were 10% molar fraction relative to SiO_2. For the catalyst Cu-Fe/SiO_2 prepared by the co-impregnation method, the SiO_2 was added into the solution of copper and iron nitrates, followed by evaporation in ambient atmosphere, and then dried at 110 °C overnight, at last calcined in static air at 350 °C for 4 h. For the catalysts Fe/Cu/SiO_2 and Cu/Fe/SiO_2 prepared by sequential impregnation method, the SiO_2 was impregnated with the aqueous solution of $Cu(NO_3)_2$ and $Fe(NO_3)_3$ by different impregnation sequence. More specifically, Cu was impregnated and calcined first followed by Fe impregnation over the Cu/SiO_2 catalyst, and Cu was impregnated second onto a calcined Fe/SiO_2, which was noted as Fe/Cu/SiO_2 and Cu/Fe/SiO_2, respectively.

* Corresponding author.
E-mail address: dsmao@sit.edu.cn (D. Mao).

http://dx.doi.org/10.1016/j.catcom.2016.07.003
1566-7367/

2.2. Catalyst testing

CO hydrogenation was performed in a fixed-bed micro reactor (made of stainless steel) with length of 350 mm and internal diameter of 5 mm. The result of preliminary experiment indicated that there were no products produced without the participation of catalysts. The catalyst (0.3 g) that diluted with inert α-alumina (0.5 g) to avoid channeling and hot spots was loaded between quartz wool and axially centered in the reactor tube, with the temperature monitored by a thermocouple close to the catalyst bed. Prior to reaction, the catalyst was heated to 300 °C (heating rate = 3 °C/min) and reduced with a H_2/N_2 mixture (50 mL/min, $V_{H2}/V_{N2} = 1:9$) for 4 h at atmospheric pressure, then cooled down to 250 °C and the reaction started as gas flow was switched to a H_2/CO mixture (30 mL/min, $V_{H2}/V_{CO} = 2:1$) at 3 MPa. All post-reactor lines and valves were heated to 150 °C for preventing the possible condensation of products. The exit products were analyzed on-line by GC (Agilent 6820) equipped with a flame ionization detector (FID) for oxygenates and hydrocarbons, and a thermal conductivity detector (TCD) for CO and CO_2. The conversion of CO was calculated based on the fraction of CO that formed carbon-containing products according to: % conversion = $(\sum n_i M_i / M_{CO}) \times 100$, where n_i is the number of carbon atoms in product i; M_i is the percentage of product i detected, and M_{CO} is the percentage of CO in the syngas feed. The selectivity of a certain product was calculated based on carbon efficiency using the formula $\% S_i = (n_i C_i / \sum n_i C_i) \times 100$, where n_i and C_i are the carbon number and molar concentration of the product i, respectively. The carbon balance was 100 ± 5%, and the margin of error was 5% for CO conversion and product selectivity.

2.3. Catalyst characterization

XRD patterns were recorded on a PANalytical X'Pert instrument using Ni β-filtered Cu K_α radiation (λ = 0.15418 nm) at 40 kV and 40 mA. Two theta angles (2θ) ranged from 10° to 70° with a scanning rate of 4°/min.

BET specific surface areas (S_{BET}), pore volumes (V_p) and average pore diameters (D_p) of the catalysts were measured by N_2 adsorption–desorption isotherms at −196 °C using a Micromeritics ASAP 2020 M + C adsorption apparatus after degassing the samples under vacuum at 200 °C for 6 h. S_{BET} was calculated using a value of 0.162 nm^2 for the cross-sectional area of the nitrogen molecule; pore volume was determined by BJH adsorption cumulative volume of pores; average pore diameter was calculated using adsorption average pore width (4 V/A by BET).

H_2 temperature-programmed reduction (H_2-TPR) was carried out in a quartz micro-reactor. Firstly, 0.05 g of the prepared catalyst was pretreated at 300 °C in N_2 flow for 1 h prior to a TPR measurement. During the TPR experiment, H_2/N_2 mixture gas with $V_{H2}/V_{N2} = 1:9$ was used at 50 mL/min and the temperature was ramped from 50 to 650 °C at a rate of 10 °C/min while the effluent gas was analyzed with a TCD.

The adsorption of CO on catalyst surface was studied using a Nicolet 6700 IR spectrometer equipped with a DRIFT (diffuse reflectance infrared Fourier transform) cell with CaF_2 windows. The sample in the cell was pretreated in H_2/N_2 (50 mL/min, $V_{H2}/V_{N2} = 1:9$) at 300 °C for 1 h, followed by N_2 stream (50 mL/min, Ultrahigh-purity) flushing at 300 °C for 0.5 h. After the temperature was dropped to 30 °C, the background was scanned in N_2 flow. Followed by introducing 0.5% CO/N_2 (50 mL/min) into the IR cell, the IR spectrum of CO adsorbed on the catalyst was recorded at 30 °C, when adsorption state remained steady. The spectral resolution was 4 cm^{-1} and the number of scans was 64.

Temperature-programmed desorption of adsorbed CO (CO-TPD) was carried out in a quartz micro-reactor. The catalyst (0.1 g) was firstly reduced for 1.5 h at 300 °C in H_2 (50 mL/min), and then cooled down to 50 °C in He flow. The next step was CO adsorption at 50 °C for 30 min until the saturation of the catalyst surface. Then the catalyst was swept with He for 1 h. Subsequently, the sample was heated in a flowing He stream (50 mL/min) up to 650 °C at a rate of 10 °C/min. The desorbed species were detected with a quadrupole mass spectrometer (QMS, Balzers Omnistar 200). MS signals at m/z = 28 (CO) and 44 (CO_2) were continuously recorded.

X-ray photoelectron spectra (XPS) were recorded on the Thermo Scientific ESCALAB 250Xi spectrometer with an Al anode for Ka (1486.6 eV) radiation. Charging effects were corrected by adjusting the binding energy of C1s peak from carbon contamination to 284.6 eV.

Table 1
Crystallite sizes and textural properties of the support and catalysts.

Sample	D_{CuO}[a] nm	$D_{Fe_2O_3}$[a] nm	D_{Cu}[b] nm	$D_{Fe_3O_4}$[b] nm	S_{BET}[a] ($m^2 \cdot g^{-1}$)	V_p[a] ($cm^3 \cdot g^{-1}$)	D_p[a] nm
$Cu\text{-}Fe/SiO_2$	16.4	8.6	21.7	16.7	208.8	0.56	10.7
$Fe/Cu/SiO_2$	19.1	5.1	23.7	14.1	178.7	0.50	11.2
$Cu/Fe/SiO_2$	20.7	12.4	26.4	20.4	212.5	0.57	10.9
SiO_2	–	–	–	–	261.4	0.89	13.7

[a] The calcined catalysts.
[b] The reduced catalysts.

3. Results and discussion

3.1. Catalyst characterization

From the XRD patterns of the calcined catalysts (Fig. S1), we can see that all the catalysts show diffraction peaks at 2θ of 35.6°, 38.8°, 48.7°, and 33.4°, corresponding to crystal CuO and α-Fe_2O_3, respectively [16]. The average crystallite sizes of CuO and Fe_2O_3 calculated by Scherrer formula are shown in Table 1. As shown, the crystallite size of CuO follows the order: $Cu\text{-}Fe/SiO_2 < Fe/Cu/SiO_2 < Cu/Fe/SiO_2$, while that of Fe_2O_3 follows the order: $Fe/Cu/SiO_2 < Cu\text{-}Fe/SiO_2 < Cu/Fe/SiO_2$.

Fig. 1 presents the XRD patterns of the reduced catalysts. The very broad peak centered at 2θ of 22.2° observed on all the catalysts can be attributed to amorphous SiO_2. Additionally, the peaks at 2θ = 43.2°, 50.7°, 74.1°; and 35.8°, 57.3°, 62.9° are ascribed to the presence of Cu and Fe_3O_4, respectively [4]. However, the peaks attributed to CuO and α-Fe_2O_3 disappeared totally. These results suggest that the CuO and α-Fe_2O_3 were respectively reduced to Cu and Fe_3O_4 after reduction. On the other hand, the change trends for the crystallite sizes of Cu and Fe_3O_4 particles over the reduced catalysts are the same as those for crystallite sizes of the CuO and α-Fe_2O_3 particles over the calcined catalysts (Table 1).

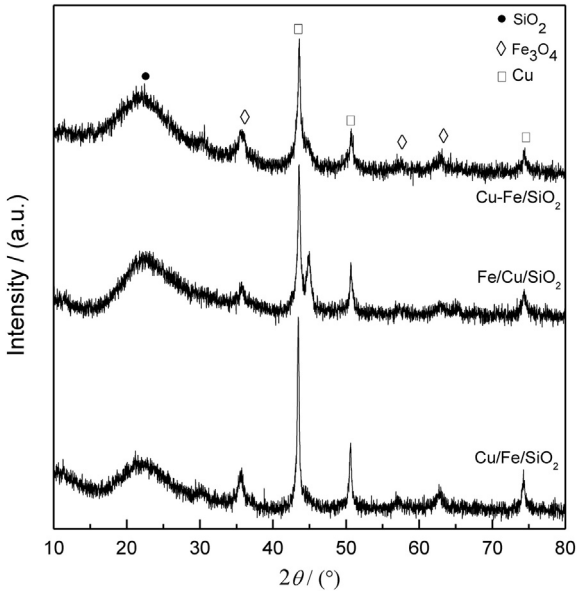

Fig. 1. XRD patterns of the reduced catalysts.

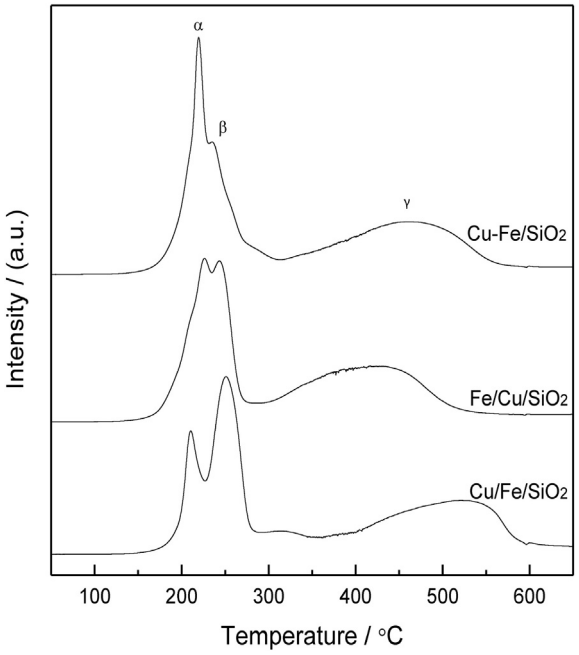

Fig. 2. H_2-TPR curves of the catalysts.

Textural parameters of the catalysts and support are also listed in Table 1. As seen, the BET surface areas, pore volumes, and average pore diameters of the catalysts are smaller than those of SiO_2 support, which can be attributed to the deposition of oxides of Cu and Fe in the pores of SiO_2 [15,21]. Particularly, the Cu-Fe/SiO_2 and Cu/Fe/SiO_2 catalysts have similar surface area and pore volume, which are larger than those of the Fe/Cu/SiO_2 catalyst.

Fig. 2 shows the H_2-TPR profiles of the catalysts. It can be seen that there are three reduction peaks (α, β and γ): the α and β peaks are assigned to the reduction of highly dispersed CuO and bulk CuO, respectively [22], while the very broad γ peak can be ascribed to the stepwise reduction of Fe_2O_3 ($Fe_2O_3 \rightarrow Fe_3O_4 \rightarrow FeO \rightarrow Fe$) [22].

It is evident from Fig. 2 that different impregnation sequences affect the reducibility of Cu and Fe oxides. Firstly, the intensity of α peak decreased in the order of Cu-Fe/SiO_2 > Fe/Cu/SiO_2 > Cu/Fe/SiO_2, while that of β peak increased in the reverse order. This phenomenon suggests that the relative content of highly dispersed CuO decreased in the order of Cu-Fe/SiO_2 > Fe/Cu/SiO_2 > Cu/Fe/SiO_2, indicating that the dispersion of CuO decreased in the same order. Secondly, the temperature for maximum of γ peak increased in the order of Fe/Cu/SiO_2 < Cu-Fe/SiO_2 < Cu/Fe/SiO_2, indicating that the crystallite size of Fe_2O_3 followed the same order, since the larger the crystallite size is, the higher the reduction temperature should be [33]. These results are in good agreement with those from XRD characterization.

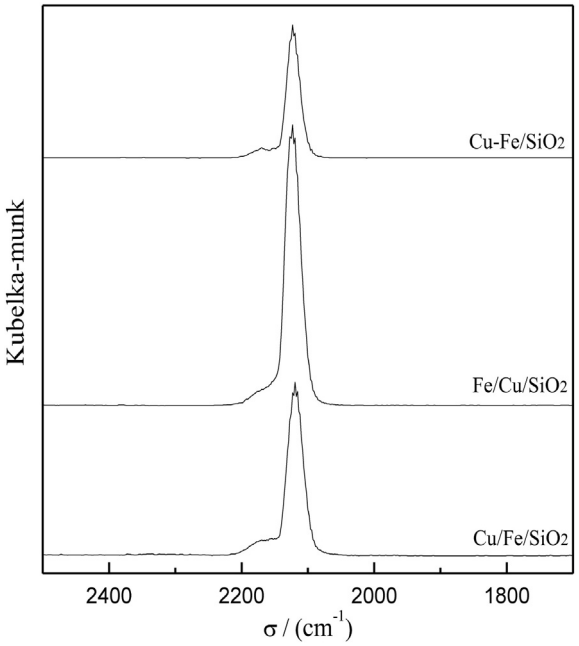

Fig. 3. IR spectra of CO chemisorbed on different catalysts.

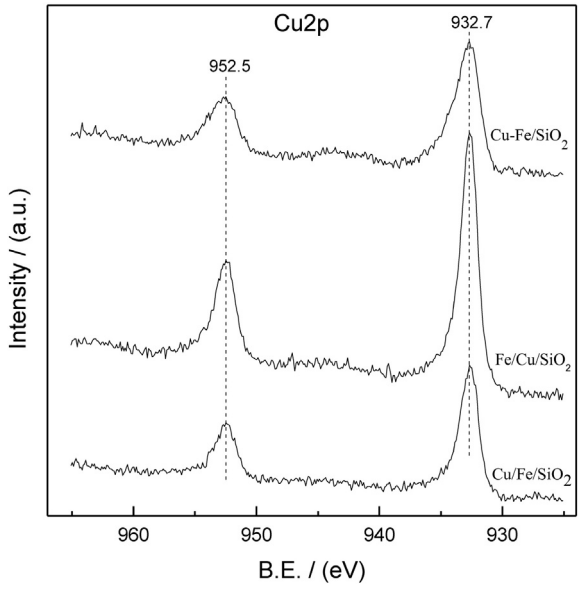

Fig. 4. XPS spectra for Cu 2p of the reduced catalysts.

Fig. 3 shows the infrared spectra of the in situ reduced catalysts after CO adsorption. A strong band at about 2120 cm^{-1} was observed over all the catalyst, which can be attributed to the CO linearly adsorbed on copper species [7,8]. The band intensity of the three catalysts follows the order: Fe/Cu/SiO_2 > Cu/Fe/SiO_2 > Cu-Fe/SiO_2, which is in agreement with the order of surface Cu content as determined by XPS (see below).

From the XPS spectra for the Cu 2p of the calcined catalysts (Fig. S2), two peaks at ~933 eV and ~953 eV attributed to the spin-obit doublet of Cu 2p are observed, which can be assigned to the binding energies of Cu $2p_{3/2}$ and Cu $2p_{1/2}$ in CuO, respectively [23]. The other two peaks on the higher binding energy side of both Cu $2p_{3/2}$ and Cu $2p_{1/2}$ are satellite structures. From the XPS spectra for the Fe 2p of the calcined catalysts (Fig. S3), the binding energies of Fe $2p_{3/2}$ and Fe $2p_{1/2}$ are at ~710 eV and ~723 eV, respectively, corresponding to Fe_2O_3 [23]. Based on these results, it can be concluded that the copper and iron species in all the calcined catalysts exist as Cu^{2+} and Fe^{3+}, respectively. This result is in accordance with that obtained by XRD study.

The XPS spectra for Cu 2p of the reduced catalysts are shown in Fig. 4. The binding energies of Cu $2p_{3/2}$ and Cu $2p_{1/2}$ are at 932.7 eV and 952.5 eV, respectively, which is the characteristic of Cu^0 [34]. The disappearance of the shake-up satellites verifies the absence of Cu^{2+} species after the reduction process [25]. The pure Cu phase on the reduced catalysts detected by the XPS is in agreement with the result of XRD (Fig. 1). On the other hand, for Cu-Fe/SiO_2 and Cu/Fe/SiO_2, the intensity of

Table 2
Surface compositions of the reduced catalysts determined by XPS.

Catalyst	Surface composition (mol %)				Cu/Fe molar ratio
	Cu	Fe	Si	O	
Cu-Fe/SiO_2	0.52	3.90	26.02	69.56	0.13
Fe/Cu/SiO_2	0.69	5.54	28.13	65.65	0.12
Cu/Fe/SiO_2	0.54	2.99	29.30	67.17	0.18

Table 3
Performance of different catalysts in CO hydrogenation.

Catalyst	CO conv. %	Selectivity %			STY_{ROH} ($g \cdot kg_{cat}^{-1} \cdot h^{-1}$)	Alcohol distribution %	
		CO_2	CH_X	ROH		CH_3OH	$C_{2+}OH$
Cu-Fe/SiO_2	13.9	16.6	59.9	23.5	90.0	67.8	32.2
Fe/Cu/SiO_2	17.6	17.9	56.0	26.1	126.6	56.3	43.7
Cu/Fe/SiO_2	15.4	12.5	51.4	36.1	153.3	62.5	37.5

Reaction conditions: 250 °C, 3.0 MPa, $V_{H2}/V_{CO} = 2$, SV = 6000 mL/($g_{cat} \cdot h$).

the Fe 2p peaks of the reduced samples (Fig. S4) was significantly enhanced in comparison with the calcined ones (Fig. S3), indicating that their surface compositions have greatly changed after reduction process.

The surface compositions of the reduced catalysts calculated from the XPS spectra are summarized in Table 2. As seen, the surface content of Cu of the catalysts follow the order of Fe/Cu/SiO_2 > Cu/Fe/SiO_2 > Cu-Fe/SiO_2, which is consistent with the result obtained by above CO-IR characterization. On the other hand, the Cu/Fe molar ratio of the Cu/Fe/SiO_2 catalyst is the largest due to its smallest surface content of Fe. This result can be due to the formation of relatively larger Fe_3O_4 particles on this catalyst as evidenced by the results of XRD (Table 1) and TPR (Fig. 2).

3.2. Catalytic performance

As shown in Table 3, the Cu-Fe/SiO_2 catalyst shows the lowest CO conversion, the selectivity of total alcohols (ROH) and higher alcohols ($C_{2+}OH$), and the space time yield (STY) of ROH. Compared with the Cu-Fe/SiO_2 catalyst, the Cu/Fe/SiO_2 and Fe/Cu/SiO_2 catalysts show better catalytic properties. The CO conversion follows the order: Fe/Cu/SiO_2 > Cu/Fe/SiO_2 > Cu-Fe/SiO_2, while the selectivity and STY of ROH follow the order: Cu/Fe/SiO_2 > Fe/Cu/SiO_2 > Cu-Fe/SiO_2. On the other hand, the highest ROH selectivity obtained on the Cu/Fe/SiO_2 catalyst is due to the lowest selectivity of the undesirable byproducts (CO_2 and CH_x). Moreover, the STY of ROH on the Cu/Fe/SiO_2 catalyst reached 153.3 $g \cdot kg_{cat}^{-1} \cdot h^{-1}$, which is 1.7 and 1.2 times larger than that of Cu-Fe/SiO_2 and Fe/Cu/SiO_2, respectively.

Based on the reaction mechanism for HAS [6,11,23,24], all the reactions involved take place on the sites of copper and iron. Therefore, the activity and selectivity of catalysts are greatly dependent on the surface contents of copper and iron. In this work, the order of CO conversion of the three catalysts (Table 3) is in agreement with that of the number of active copper species, which contribute to CO adsorption as evidenced by the result of CO-IR analysis (Fig. 3). Similar result was also reported previously [22,35]. On the other hand, the synthesis of alcohols including methanol and higher alcohols requires the participation of copper, while the synthesis of hydrocarbons only requires the participation of iron. Thus, the higher ratio of Cu/Fe will benefit for the formation of alcohols; on the contrary, the higher ratio of Fe/Cu will benefit for the formation of hydrocarbons. If this hypothesis holds, the Cu/Fe/SiO_2 catalyst with the highest Cu/Fe molar ratio should have the highest ROH selectivity and the lowest CH_x selectivity, which is in perfect agreement with the results obtained by catalyst testing (Table 3).

4. Conclusion

The effects of impregnation sequences on the properties of Cu-Fe/SiO_2 catalysts for the higher alcohols synthesis were investigated. The results indicate that different positions of copper and iron in the catalysts significantly influence the activities of Cu-Fe/SiO_2 catalyst. The highest selectivity and STY of ROH were obtained on Cu/Fe/SiO_2, in which Fe was impregnated and calcined first followed by Cu impregnation and calcination. However, the highest CO conversion was obtained on Fe/Cu/SiO_2 catalyst, in which Cu was impregnated and calcined first followed by Fe impregnation and calcination. The high CO conversion can be attributed to the high surface content of Cu, while the high ROH selectivity can be attributed to the high ratio of surface contents of Cu to Fe.

Acknowledgment

The authors acknowledge financial supports from the Science and Technology Commission of Shanghai Municipality (13ZR1461900, 08520513600).

Appendix A. Supplementary data

Supplementary data to this article can be found online at http://dx.doi.org/10.1016/j.catcom.2016.07.003.

References

[1] K.G. Fang, D.B. Li, M.G. Lin, M.L. Xiang, W. Wei, Y.H. Sun, Catal. Today 147 (2009) 133–138.
[2] V.R. Surisetty, A.K. Dalai, J. Kozinski, Appl. Catal. A Gen. 404 (2011) 1–11.
[3] M. Gupta, M.L. Smith, J.J. Spivey, ACS Catal. 1 (2011) 641–656.
[4] K. Xiao, X. Qi, Z. Bao, X. Wang, L. Zhong, K. Fang, M. Lin, Y. Sun, Catal. Sci. Technol. 3 (2013) 1591–1602.
[5] M.Y. Ding, M.H. Qiu, J.G. Liu, Y.P. Li, T.J. Wang, L.L. Ma, Fuel 109 (2013) 21–27.
[6] H. Guo, H. Zhang, F. Peng, H. Yang, L. Xiong, C. Wang, C. Huang, X. Chen, L. Ma, Appl. Catal. A Gen. 503 (2015) 51–61.
[7] R. Xu, C. Yang, W. Wei, W. Li, Y. Sun, T. Hu, J. Mol. Catal. A Chem. 221 (2004) 51–58.
[8] R. Xu, Z.Y. Ma, C. Yang, W. Wei, Y.H. Sun, React. Kinet. Catal. Lett. 81 (2004) 91–98.
[9] M. Lin, K. Fang, D. Li, Y. Sun, Catal. Commun. 9 (2008) 1869–1873.
[10] Z.H. Bao, K. Xiao, X.Z. Qi, X.X. Wang, L.S. Zhong, K.G. Fang, M.G. Lin, Y.H. Sun, J. Energy Chem. 22 (2013) 107–113.
[11] K. Xiao, Z. Bao, X. Qin, X. Wang, L. Zhong, M. Lin, K. Fang, Y. Sun, Catal. Commun. 40 (2013) 154–157.
[12] K. Xiao, Z. Bao, X. Qin, X. Wang, L. Zhong, K. Fang, M. Lin, Y. Sun, J. Mol. Catal. A Chem. 378 (2013) 319–325.
[13] M.Y. Ding, J.G. Liu, Q. Zhang, N. Tsubaki, T.J. Wang, L.L. Ma, Catal. Commun. 28 (2012) 138–142.
[14] J.G. Liu, M.Y. Ding, T.J. Wang, L.L. Ma, Acta Phys. Chim. Sin. 28 (2012) 1964–1970.
[15] J.G. Liu, M.Y. Ding, T.J. Wang, L.L. Ma, Pet. Process. Petrochem. 44 (2013) 22–27.
[16] M.Y. Ding, J.L. Tu, J.G. Liu, N. Tsubaki, T.J. Wang, L.L. Ma, Catal. Today 234 (2014) 278–284.
[17] Y. Su, Y. Wang, Z. Liu, J. Nat. Gas Chem. 17 (2008) 327–331.
[18] H. Zhang, X. Yang, L. Zhou, Y. Su, Z. Liu, J. Nat. Gas Chem. 18 (2009) 337–340.
[19] X. Yang, Y. Wei, Y. Su, L. Zhou, Fuel Process. Technol. 91 (2010) 1168–1173.
[20] D.S. Mao, Q.S. Guo, J. Yu, L.P. Han, G.Z. Lu, Acta Phys. Chim. Sin. 27 (2011) 2639–2645.
[21] Q.S. Guo, D.S. Mao, J. Yu, L.P. Han, J. Fuel Chem. Technol. 40 (2012) 1103–1107.
[22] R.L. Lu, D.S. Mao, J. Yu, Q.S. Guo, J. Ind. Eng. Chem. 25 (2014) 338–343.
[23] Y.W. Lu, F. Yu, J. Hu, J. Liu, Appl. Catal. A Gen. 429-430 (2012) 48–58.
[24] Y. Lu, B. Cao, F. Yu, J. Liu, Z. Bao, J. Gao, ChemCatChem 6 (2014) 473–478.
[25] W. Gao, Y.F. Zhao, J.M. Liu, Q.W. Huang, S. He, C.M. Li, J.W. Zhao, M. Wei, Catal. Sci. Technol. 3 (2013) 1324–1332.
[26] J.M. Beiramar, A. Griboval-Constant, A.Y. Khodakov, ChemCatChem 6 (2014) 1788–1793.
[27] H. Zhang, W. Chu, H.Y. Xu, J. Zhou, Fuel 89 (2010) 3127–3131.
[28] S. Deng, W. Chu, H. Xu, L. Shi, L. Huang, J. Nat. Gas Chem. 17 (2008) 369–373.
[29] J.J. Wang, Q.H. Zhang, Y. Wang, Catal. Today 171 (2009) 257–265.
[30] J. Yu, D.S. Mao, L.P. Han, Q.S. Guo, G.Z. Lu, Fuel Process. Technol. 112 (2013) 100–105.
[31] A.L. Borer, R. Prins, J.G. Goodwin, K.P. Dejong, A.T. Bell, F. Solymosi, R.D. Gonzalez, D.C. Koningsberger, F. Pinna, P. Johnston, V. Ponec, K.C. Waugh, J.W.E. Coenen, M. Ichikawa, K. Klier, M. Schmal, W.M.H. Sachtler, Stud. Surf. Sci. Catal. 75 (1993) 765–779.
[32] W. Liu, S. Wang, S. Wang, Appl. Catal. A Gen. 510 (2016) 227–232.
[33] X.M. Guo, D.S. Mao, G.Z. Lu, S. Wang, G.S. Wu, J. Catal. 271 (2010) 178–185.
[34] M. Zhang, Z. Liu, G. Lin, H. Zhang, Appl. Catal. A Gen. 451 (2013) 28–35.
[35] V. Mahdavi, M.H. Peyrovi, M. Islami, J.Y. Mehr, Appl. Catal. A Gen. 281 (2005) 259–265.